Contents list available at CBIORE journal website

International Journal of Renewable Energy Development

Journal homepage: https://ijred.cbiore.id

Research Article

Electrochemical properties of porous carbon derived from polymer waste

Beifang Wang[1,*] and Xiangmeng Guo[2]

[1] School of Life Science and Health Engineering, Luoyang Institute of Science and Technology, Luoyang, 471023, China

[2] College of Life Sciences, Luoyang Normal University, Luoyang, 471023, China

Abstract. The exponential accumulation of non-degradable polymer waste poses a severe environmental challenge. In order to achieve high-value recycling and meet the demand for advanced energy storage, this study converts various polymer wastes into high-performance porous carbon (PC) electrode materials for supercapacitors. The waste hollow fiber filter (HFC), polyurethane shoe material (PUC) and PET foam (PFC) were converted into PC with a customized morphological framework through pre carbonization combined with high temperature KOH chemical activation. The results showed that HFC activated with 1:4 KOH and CAR at 750 ℃ achieved 2934 $m^2 \cdot g^{-1}$ specific surface area (SSA) and synergistic in situ N/O self-doping. This structural optimization provides an excellent specific capacitance (SC) of 297 $F \cdot g^{-1}$ at 1$A \cdot g^{-1}$. Dynamics analysis shows that enriched Faraday redox sites and graded porosity result in an ultra-low charge transfer resistance of 0.22 Ω and a high capacitance control contribution of 84.7% at 20 $mV \cdot s^{-1}$. In addition, PUC activated at 850 ℃ exhibited a coral like rigid 3D skeleton, producing an SSA of 1467 $m^2 \cdot g^{-1}$, a capacity retention rate (CRR) of 85.4% at 10 $a \cdot g^{-1}$, and an internal resistance as low as 0.97 Ω. PFC (CAR 1:4) activated at 750 ℃ forms a honeycomb structure, providing 2281 $m^2 \cdot g^{-1}$ SSA and 296 $F \cdot g^{-1}$, with excellent electrolyte diffusion kinetics. This work elucidates the relationship between precursor topology and pore evolution, providing a sustainable approach for the next generation of energy storage devices.

Keywords: Polymer waste; Porous carbon; Potassium hydroxide activation; Supercapacitor; Electrochemical performance

Received: 17th April 2026; Revised: 19th August 2026; Accepted: 1st Sept 2026; Available online: 21st Sept 2026

1. Introduction

Currently, the use of polymer materials including hollow fiber filters, polyurethane shoe materials, and polyethylene terephthalate (PET) foam has increased dramatically. This type of waste polymer is difficult to degrade naturally, and its large accumulation can easily cause serious environmental pollution (Singh, Sharma & Dhanorkar 2023). There is an urgent need to explore effective ways of high-value recycling and energy utilization of polymer waste. Meanwhile, if waste polymer materials can be transformed into high-performance porous carbon (PC) electrode materials for supercapacitors, it can not only solve the environmental and resource crisis, but also significantly reduce the preparation cost of energy storage devices (Li *et al.* 2023). In the current research on advanced PC materials, the core challenge is how to coordinate the contradiction among pore engineering, heteroatom doping strategy, and electrochemical performance. In terms of pore engineering, although MOF derived or template methods can achieve high specific surface area, these processes not only rely on complex templates but also easily lead to product aggregation and skeleton collapse during subsequent High-Temperature Activation (HTA), resulting in extremely high interfacial contact resistance (Li *et al.* 2024; Sun *et al.* 2024). On the contrary, although traditional biomass or fossil based carbon materials have controllable processes, their microporous distribution is single and lacks a multi-level pore structure, resulting in slow electrolyte ion transport kinetics under high-rate charge and discharge, making it difficult to achieve capacitance breakthroughs beyond commercial activated carbon (Benoy *et al.* 2024; Ashok Kumar *et al.* 2023). Previous studies have often relied on strong acid oxidation or surface post doping for the contribution of impurity doping and pseudo capacitance (Niu *et al.* 2023; Ding, Xue&Hu 2024). Although this type of method can introduce oxygen nitrogen functional groups to enhance pseudo capacitance, the intense strong oxidation process can damage the long-range ordered conductive framework of carbon materials, resulting in a significant decrease in intrinsic electronic conductivity and a severe increase in internal resistance under high current density loads. Therefore, developing a method that can achieve hierarchical pore engineering through precursor topology control and retain heteroatom doping through in-situ strategy has become the key to improving the electrochemical performance of polymer derived PC.

Overall, the current literature on the conversion of waste polymers into PCs is mostly focused on homogeneous plastics from a single source, often lacking a systematic comparison of the pore evolution regulation mechanisms of different intrinsic heteroatom frameworks. Although KOH activation has been

* Corresponding author
Email: Wangbeif1016@163.com (B. Wang)

https://doi.org/10.61435/ijred.2026.62638
ISSN: 2252-4940/© 2026.The Author(s). Published by CBIORE

widely used in preparing PC, existing research generally considers it as a universal pore forming method and pays less attention to the differential effects of precursor macromolecular topology on activation reaction kinetics (Zhou *et al.* 2026; Blanchard *et al.* 2024). To break through the bottleneck of high proportion of micropores and slow ion mass transfer kinetics in traditional biomass-based PC, three representative physical forms and unique chemical heterogeneity of polymer waste were selected as precursors for the study. The inherent high aspect ratio tubular network of discarded hollow fiber carbon (HFC) can serve as a natural channel for gas escape during pyrolysis, helping to form a long-range interpenetrating three-dimensional porous skeleton and promoting macroscopic convective mass transfer under high current density (Li *et al.* 2025; Taer *et al.* 2025). Waste polyurethane carbon (PUC) shoe materials, as nitrogen rich polymers, release nitrogen-containing gases in situ through their amino ester bonds during thermal degradation, acting as self-pore forming agents. The ester-based structure with high oxygen content in waste PET foam carbon (PFC) can provide abundant hydrophilic sites before chemical activation, and its porous cell structure is conducive to constructing honeycomb interconnection porous structure with high mechanical strength (Chen *et al.* 2025; Wang *et al.* 2025). A strategy of pre-carbonization combined with high-temperature potassium hydroxide (KOH) chemical activation has been proposed to convert PC derived from HFC, PUC, and PFC into high-performance supercapacitor (HPS) PCs, filling the theoretical gap in the multi-element high-value utilization of polymer waste. This paper aims to offer a feasible path for the design of HPS electrode materials. The innovation lies in utilizing the inherent morphological characteristics of waste polymers and evolving in situ a coral-like or honeycomb-like rigid 3D interpenetrating mesh skeleton through intense etching by activators, which is conducive to broadening the double-layer energy storage interface. This study directly achieves in-situ self-doping of nitrogen (N) and oxygen (O) heteroatoms through the HTA process. This process enriches carbonyl and quinone groups with extremely high electrochemical activity on the carbon surface and achieves efficient synergy between the electric double-layer and pseudo capacitance.

2. Experimental materials

2.1 Reagents, Materials, and Instruments

The main polymer waste materials used in the experiment include waste hollow fiber filter membrane recycled by the local water treatment plant, waste polyurethane soft soled shoes collected by waste recycling points, and waste PET foam recycled from logistics packaging waste (Ma *et al.* 2024). In terms of chemical reagents and materials, analytical grade potassium hydroxide (China National Pharmaceutical Group Chemical Reagent Co., Ltd.), concentrated hydrochloric acid (Guangzhou Chemical Reagent Factory), anhydrous ethanol (Tianjin Fuyu Fine Chemical Co., Ltd.), and analytical grade polytetrafluoroethylene (PTFE, Shanghai Aladdin Biochemical Technology Co., Ltd.) with a mass fraction of 60% were mainly used. In addition, battery grade acetylene black (Shenzhen Kejing Zhida Technology Co., Ltd.) and 110 PPI (435 g/m ²) foam nickel (Changsha Liyuan New Material Co., Ltd.) were also used. The water for the experiment was ultra-pure water provided by the laboratory. In the process of material preparation and characterization testing, the research mainly relies on high-temperature tube furnace (TL1200) for material sintering and uses electrochemical workstation (CS350) for performance testing. Cold field emission scanning electron microscope (GeminiSEM 300), field emission transmission electron microscope (JEM-2100F), X-ray photoelectron spectrometer (AXIS Ultra DLD), and specific surface area and porosity analyzer (Autosorb-iQ) and other analytical instruments are used to characterize the microstructure and pore structure of the samples.

2.2 Methodologies

2.2.1 Preparation of PC materials

When preparing PCs, this paper uniformly uses pre-carbonization combined with KOH HTA method to convert three waste polymer materials into PCs. Fig.1 shows the specific preparation flowchart.

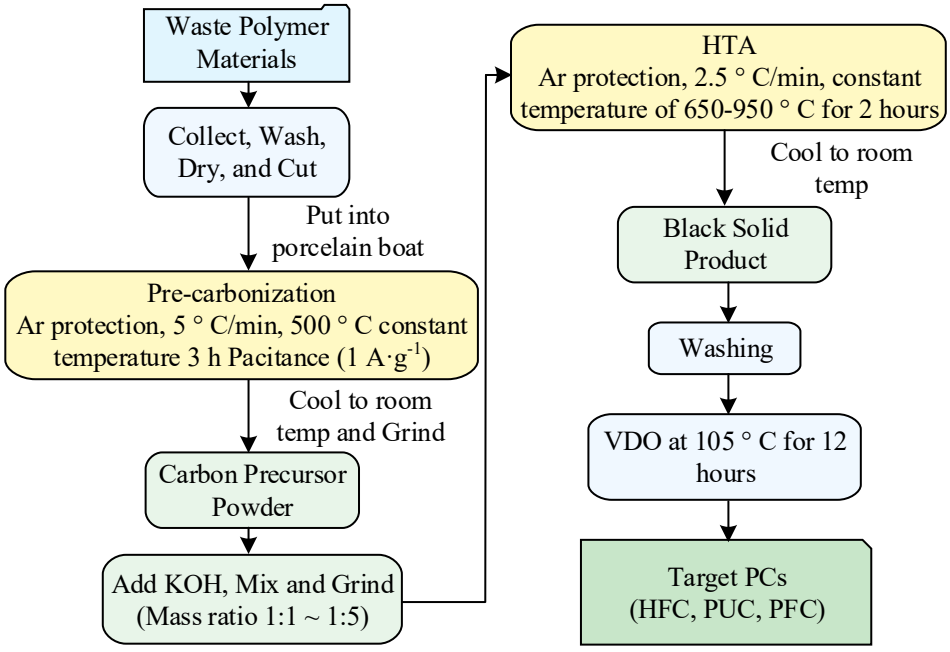

Fig.1 Preparation process of PCs

In Fig.1, the preparation includes three stages. The first is the pre-carbonization stage of the carbon precursor. The collected, washed, dried, and shredded polymer waste needs to be placed in a porcelain boat and a HTTF. In an atmosphere protected by high-purity argon (Ar), the temp is raised to 500 ℃ at a rate of 5 ℃/min and roasted at a constant temp for 3 hours. After natural cooling, the carbon precursor powder is obtained by grinding (Yue, Lu & Liu 2025). The three types of waste polymers collected were washed alternately with ultrapure water and anhydrous ethanol three times to remove surface impurities, dried at 80 ℃ for 24 hours, and then sheared and crushed using a mechanical crusher. To ensure the consistency of precursor reaction kinetics, the crushed particles were classified and screened through a standard sieve, with an average particle size distribution (D50) controlled at 45±5 μm. During the pre-carbonization process, the constant flow rate of high-purity argon gas (99.999%) in the tube furnace is adjusted to 150 sccm, and continuous ventilation is carried out for 30 minutes before heating to completely expel residual air in the furnace. Subsequently, the obtained carbon precursor and the activator KOH are mixed and ground at a mass ratio of 1:1 to 1:5, then placed into a tube furnace again, raised to the target temp (650, 750, 850, or 950, in ℃) at a heating rate of 2.5 ℃/min under Ar gas protection and activated at a constant temp for 2 h. After HTA and natural cooling, transfer the black solid product to a beaker, add 1 M HCl solution, and continue magnetic stirring at 60 ℃ for 4 hours to ensure complete dissolution of residual metal potassium, potassium carbonate, and inorganic by-products. Subsequently, a polytetrafluoroethylene (PTFE) microporous membrane with a pore size of 0.22 μm was used for vacuum filtration. The filter cake was repeatedly washed with hot ultrapure water until the conductivity of the effluent stabilized below 10 μS/cm and the pH value remained neutral. Finally, the neutral filter cake was placed in a 105°C vacuum drying oven and dried at a constant temperature for 12 hours.
To reduce the carbon footprint and environmental impact of KOH activation process, a closed-loop recovery scheme was adopted in the study: the activated product was washed with deionized water multiple times. The filtrate was recovered by vacuum evaporation to recover excess KOH, with a recovery rate of over 88.5%. By-products such as H_2 generated during the activation process were collected and used for fuel supply in the pre-carbonization stage, achieving energy self-consistency within the process.

2.2.2 Structural and micromorphological characterization

To explore the micromorphology, pore evolution rules and surface chemical microenvironment of the prepared PCs, this study carries out a series of physical and chemical characterizations. The experiment mainly uses SEM and TEM to observe the morphological characteristics and the internal 3D interconnected pore network. SSA and pore analyzer are used to obtain the N_2 adsorption and desorption isotherm of the sample at 77 K liquid N temp (Tian *et al.* 2024). The total SSA is calculated through the BET equation, and the volume ratio and pore size distribution of micropores and mesopores are calculated by combining the t-plot method and the NLDFT/BJH model (Wang *et al.* 2025). In addition, this study uses XPS to decide the elemental composition of the material surface, and performs peak fitting on the high-resolution characteristic spectra (C 1s, N 1s, and O 1s) to quantify the relative percentages of different chemical binding states.

2.2.3 Preparation of working electrode

Before conducting electrochemical energy storage performance testing, the working electrode for testing needs to be prepared. In the experiment, 4 mg of the prepared PC material is weighed as the active material in a 8:1:1 mass ratio. An appropriate amount of absolute ethanol is added to an agate mortar to prepare a uniform, viscous slurry. Subsequently, the slurry is evenly coated on the pretreated nickel foam current collector, using a size of 1 cm × 1 cm. After the coating is completed, the pole piece is placed in a VDO at 80 ℃ for 10 h. After natural cooling, it is pressed on a DTP at a 10 MPa pressure for 1 min to tightly combine the active material with the nickel foam, thus preparing the working electrode.

2.2.4 Electrochemical performance testing

All electrochemical tests are completed on the CS350 electrochemical workstation, and the standard three-electrode test system is used for evaluation. A 6 M KOH aqueous solution is utilized as the electrolyte, a platinum electrode with an area of 1.5 cm^2 is taken as the counter electrode, and a calomel electrode is adopted as the reference electrode. Specific test items mainly include cyclic voltammetry testing and galvanostatic charge and discharge (GCD) testing. The current density range is 1 $A{\cdot}g^{-1}$~20 $A{\cdot}g^{-1}$. An electrochemical AC impedance test is conducted, and the internal resistance Rs and charge transfer resistance Rct of the material are examined by setting a frequency range of 0.01 Hz~100 kHz and an AC disturbance amplitude of 5 mV. Finally, a long cycle life test of 10,000 times of GCD is performed to assess the energy storage stability of the electrode. According to the GCD curve, the mass SC C_{m1} of the working electrode is calculated by Equation (1) (Kushwaha *et al.* 2024).

$$C_{m1} = \frac{I \times \Delta t}{m \times U} \tag{1}$$

In Equation (1), I means the discharge current set for the test. Δt denotes the time taken for discharge. m indicates the mass of active material loaded on the pole piece. U is the effective potential window when discharging. According to the cyclic voltammetry curve, the mass SC of the material is shown in Equation (2) (Ahmad *et al.* 2023).

$$C_{m2} = \frac{\int IdU}{2 \times v \times m \times U} \tag{2}$$

In Equation (2), v is the scan rate of the cyclic voltammetry test. To assess the energy storage potential in actual devices, the specific energy/power densities (E_m and P_m) are given in Equation (3) (Ren *et al.* 2023).

$$\begin{cases} E_m = \dfrac{1}{2 \times 3.6} C_m \times U^2 \\ P_m = \dfrac{E_m \times 3600}{\Delta t} \end{cases} \tag{3}$$

To quantitatively evaluate the electrochemical kinetics inside the electrode, the Dunns method is used to separate the total response current A into capacitance-controlled contribution A

Table 1
Influence of activation dynamics parameters on the evolution of PC pore structure

Heating rate (℃/min)	Activation time (h)	Specific surface area ($m^2 \cdot g^{-1}$)	Total pore volume ($cm^3 \cdot g^{-1}$)
1.0	2	2685	1.31
2.5	1	1850	0.84
2.5	2	2934	1.48
2.5	3	2115	1.62
5.0	2	1680	0.95

and diffusion controlled contribution A. The calculation is shown in Equation (4).

$$i(V) = k_1 v + k_2 v^{1/2} \tag{4}$$

In Equation (4), v is the scanning rate. k_1 and k_2 are constant. By linearly fitting $i(V)/v^{1/2}$ and $v^{1/2}$ at different scanning rates, the contribution ratio of capacitance control process and diffusion control process can be quantitatively separated by slope and intercept, thus clarifying the actual electrochemical proportion of pseudocapacitance.

3. Analysis of experimental results

3.1 Pre optimization of activation process kinetics parameters

Before delving into the pore evolution laws of three types of waste polymer precursors, the study first uses HFC as a model precursor and conducted a full matrix pre-optimization evaluation of activation kinetics parameters. The experimental system investigates the comprehensive effects of different heating rates (1.0, 2.5, and 5.0 ℃/min) and activation durations (1, 2, and 3 h) on the evolution of porous structures. The specific data are shown in Table 1. When the heating rate is 5.0 ℃/min, intense local chemical gasification reactions cause perforation of pore walls and collapse of the skeleton, resulting in a decrease in specific surface area to 1680 $m^2 \cdot g^{-1}$. However, 1.0 ℃/min leads to excessive energy consumption and lengthy process cycles. In terms of activation time, the constant temperature activation energy of 2 hours ensures sufficient redox reaction between KOH and carbon skeleton. If extended to 3 hours, the microporous structure is converted into ineffective macropores due to excessive etching, resulting in a reduction in the specific surface area. Therefore, the study ultimately determines that a heating rate of 2.5 ℃/min and an activation duration of 2 hours are the globally optimal process parameters.

3.2 Structure analysis of HFC

3.2.1 Pore structure and surface chemistry

To deeply analyze the pore evolution, this study compares the volume ratio of micropores and mesopores at different temps, as shown in Fig.2. In Fig.2(a), the carbonization temp plays a decisive role in the SSA and total pore volume (TPV) of PC. When the carbonization temp is 650℃, the SSA of HFC-600 is only 856 $m^2 \cdot g^{-1}$, and the TPV is only 0.42 $cm^3 \cdot g^{-1}$. As the temp grows to 750℃, the etching effect of KOH on the carbon skeleton reaches its optimal state, the SSA of HFC-750 increases to 2934 $m^2 \cdot g^{-1}$, and the TPV reaches as high as 1.48 $cm^3 \cdot g^{-1}$. When the temp further grows to 950 ℃, the SSA of HFC-950 drops significantly to 1701 $m^2 \cdot g^{-1}$. In Fig.2(b), at 650℃, the pores of the material are mainly micropores, with very few mesopores. At 750 ℃, the micropore/mesopore volumes are 0.98 $cm^3 \cdot g^{-1}$ and 0.50 $cm^3 \cdot g^{-1}$. As the temp continues to grow, the micropore volume decreases significantly, and the mesopore volume increases slightly. In summary, at 750 ℃, the pore expansion effect of HFC materials is optimal, and the multi-level pore size distribution is the most reasonable.

To further reveal the advantages of the electrochemical performance of HFC-750 (1:4), the N_2 adsorption desorption isotherms and pore size distribution are analyzed, as shown in Fig.3. In Fig.3 (a), the material exhibits typical I/IV type composite isotherm characteristics. In the low-pressure region (P/P0<0.1), there is a non-linear increase in N_2 adsorption capacity. In the medium to high-pressure region (P/P0=0.45~0.9), there is a clear H4 hysteresis loop in the isotherm, confirming the existence of narrow slit mesopores. From the perspective of physical and chemical kinetics, this hysteresis behavior reflects the geometric steric hindrance effect of mesoporous size limitations on electrolyte ion transport during capillary condensation and desorption processes. From Fig.3 (b), the material exhibits a significant microporous main peak at approximately 0.8 nm, effectively providing a high

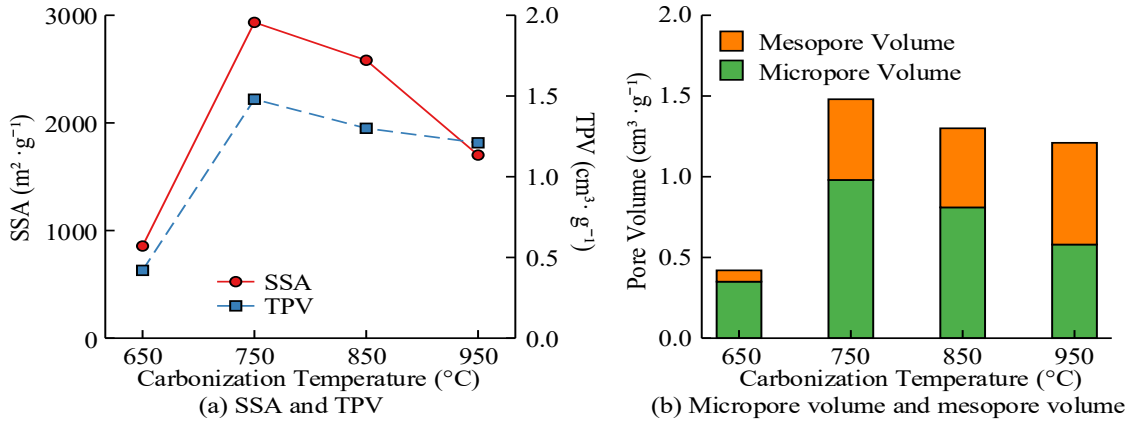

Fig.2 Multidimensional parameters of pore structure of HFC series PC

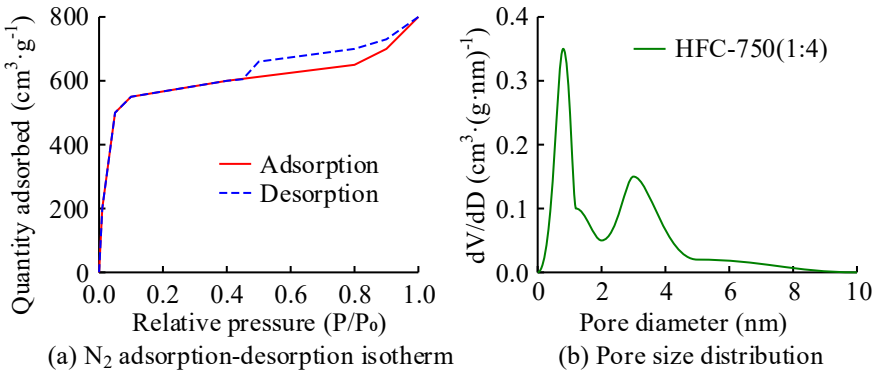

(a) N_2 adsorption-desorption isotherm (b) Pore size distribution

Fig.3 N_2 adsorption desorption isotherms and pore size distribution

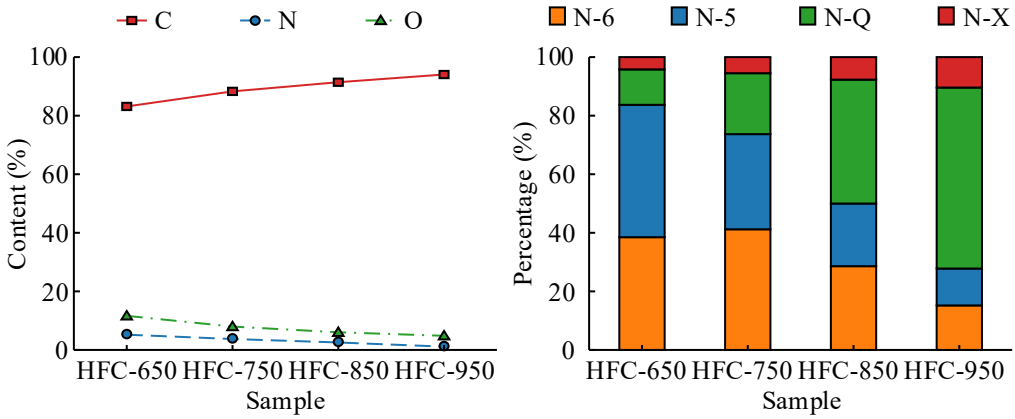

(a) Trend chart of relative content changes of C/N/O elements (b) Stacked bar chart mainly containing the proportion of N configurations

Fig.4 XPS testing of HFC series PC

specific surface area. Meanwhile, there are broad mesoporous peaks distributed at 2-4 nm. This structural configuration effectively alleviates the diffusion restriction effect of ions inside the electrode, reduces the equivalent series resistance, and ensures that HFC-750 (1:4) can still achieve fast ion transport and efficient capacitor output under high current density loads. This study then carries out XPS test analysis, as shown in Fig.4. The experiment shows that the material retains 3.73% N and 7.98% O content at 750 ℃. Quantitative analysis shows that the total proportion of pyridine nitrogen (N-6) and pyrrole/pyridone nitrogen (N-5) is 53.8%. According to impedance fitting parameters, these defect sites reduce the charge transfer resistance by about 35% compared to pure carbon materials, significantly enhancing the adsorption affinity of interface ions. In the O 1s spectrum, the carbonyl group (C=O) accounts for 41.5%. As a typical Faraday redox active site, it provides approximately 22% of the specific capacitance contribution to the material. In addition, as the heat treatment temperature increases, the proportion of quaternary ammonium nitrogen (NQ) with strong thermal stability rises to 61.8% at 950 ℃. Although it improves the conductivity of the skeleton, the lack of Faraday electrochemical activity leads to a decrease in the total specific capacitance. In summary, the coexistence of N-6 and C=O sites at 750 ℃ enhances the double-layer and pseudocapacitive energy storage mechanism of the material, achieving the optimal balance between high conductivity and high active site density.

3.2.2 Electrochemical performance evaluation

This study further draws the rate attenuation curve and impedance comparison chart under various preparation environments, as exhibited in Fig.5. In Fig.5(a), as the current density gradually rises from 1~20 $A \cdot g^{-1}$, the SC of all HFC series samples decreases. The HFC-750 (1:4) sample has the best performance. It has the highest starting capacitance at 1 $A \cdot g^{-1}$, reaching 297 $F \cdot g^{-1}$, and the gentlest curve attenuation slope. Under an ultra-high current load of 20 $A \cdot g^{-1}$, the capacity is 239 $F \cdot g^{-1}$. This shows that a higher activator ratio effectively widens the internal pores. In Fig.5(b), ESR represents the intrinsic conductivity of the material and the contact resistance between the electrode material and the current collector. The ESR of the HFC-750 system sample is generally low, only 0.73 Ω at the 1:3 ratio, indicating that 750℃ is the best balance point between the formation of graphitized conductive network and the maintenance of porous structure. Rct reflects the resistance of ions to adsorption and desorption and Faradaic redox reaction on the electrode surface. The Rct of HFC-750 (1:4) is only 0.22 Ω, indicating that the heteroatom sites retained on its surface can effectively interact with the electrolyte. This excellent electrochemical kinetics performance is directly attributed to

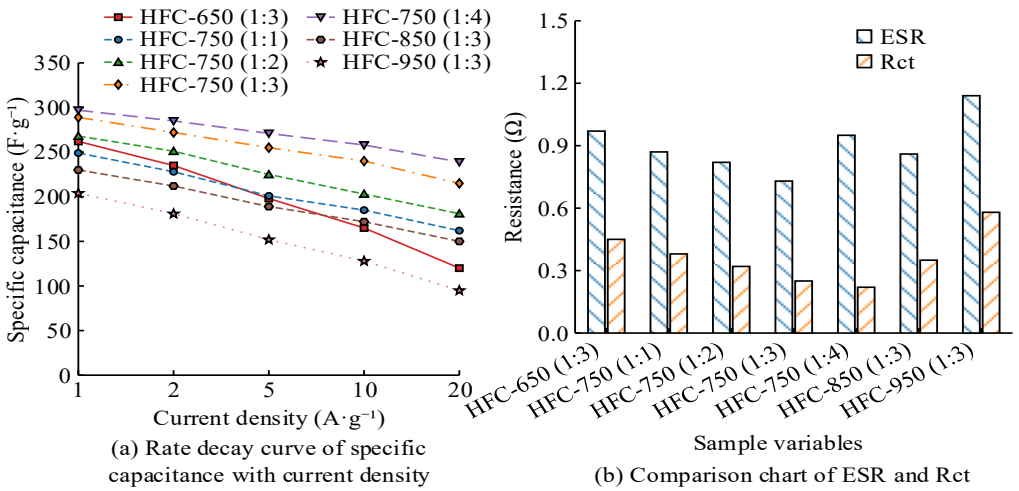

(a) Rate decay curve of specific capacitance with current density (b) Comparison chart of ESR and Rct

Fig.5 Electrochemical properties of HFC series PC

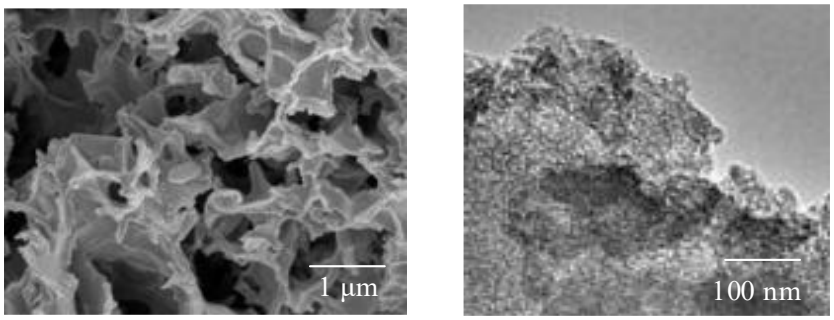

(a) SEM image (b) TEM image

Fig.6 SEM and TEM images of HFC-750 (1:4)

the optimized ion transport by the controlled multi-level pore structure. Through the correlation analysis between pore size distribution and electrochemical impedance data, it can be concluded that the interconnected network composed of mesopores formed inside HFC-750 (1:4) provides a low impedance high-speed channel for the rapid migration of electrolyte ions, effectively improving the electrolyte accessibility in the microporous region. Specifically, micropores provide a high-capacity specific surface area for charge adsorption, while mesopores shorten the average path length for ions to diffuse from the electrolyte to the inner surface of micropores, thereby reducing diffusion polarization under high current loads. In summary, a carbonization temp of 750°C and an activation mass ratio of 1:4 is the optimal process.

Fig.6 is the SEM image and TEM image of HFC-750 (1:4). The SEM image shows that the HFC-750 (1:4) material exhibits an irregular 3D interpenetrating network skeleton morphology, which can expand the effective SSA and reduce the diffusion resistance of electrolyte ions (DR-EI). Combined with the TEM image, the HFC-750 (1:4) substrate shows obvious light transmittance, and its interior is densely covered with fine spots of alternating light and dark spots, confirming that the material skeleton contains a rich micro-nano porous structure. To further reveal the interface charge transfer behavior and ion diffusion kinetics, the Nyquist plot is fitted using an $R_s(Q_{dl}(R_{ct}W))$ equivalent circuit model. The key impedance parameters of each sample are shown in Table 2. The R_{ct} of HFC-750 (1:4) is only 0.22 Ω, which is about 85% lower than that of the control sample, proving that the conductive network constructed by in-situ impurity doping significantly reduces the charge transfer energy barrier. In addition, by calculating the linear relationship between the real part of impedance in the low-frequency region and the inverse square root of frequency, the ion diffusion coefficient of HFC-750 (1:4) is 4.80×10-11 $cm^2 \cdot s^{-1}$. This result quantitatively confirms that the multi-level pore structure provides a high-speed transport channel for ions, effectively shortening the diffusion path of ions inside the solid, and endowing the material with excellent rate performance.

3.3 Structure analysis of PUC

3.3.1 Pore structure and surface chemistry

In Fig.7(a), as the carbonization temp rises from 650 to 950 °C, the SSA of PUC series samples first increases and then decreases, reaching a peak of 1,467 $m^2 \cdot g^{-1}$ at 850 °C. When the temp continues to grow to 950 °C, excessive ablation causes the hole wall to collapse, and the SSA drops back to 1,383 $m^2 \cdot g^{-1}$. The micropore ratio (V_{micro}/V_{total}) drops from 88.6% at 650 °C to 62.1% at 950 °C, indicating that high temp causes some micropores to gradually burn through and expand into mesopores. In Fig.7(b), the micropore volume remains at a high level from 750 °C to 850 °C, about 0.50 $cm^3 \cdot g^{-1}$, and then decreases significantly at 950°C. 850°C is the optimal temp for the development of pores in PUC-derived PC.

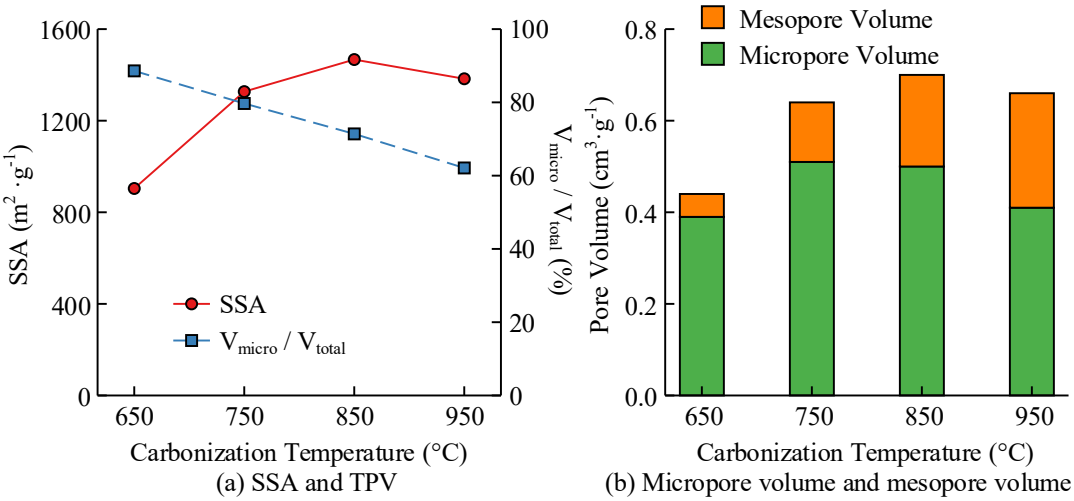

Fig.7 The influence of carbonization temp on the pore architecture of PUC series PC

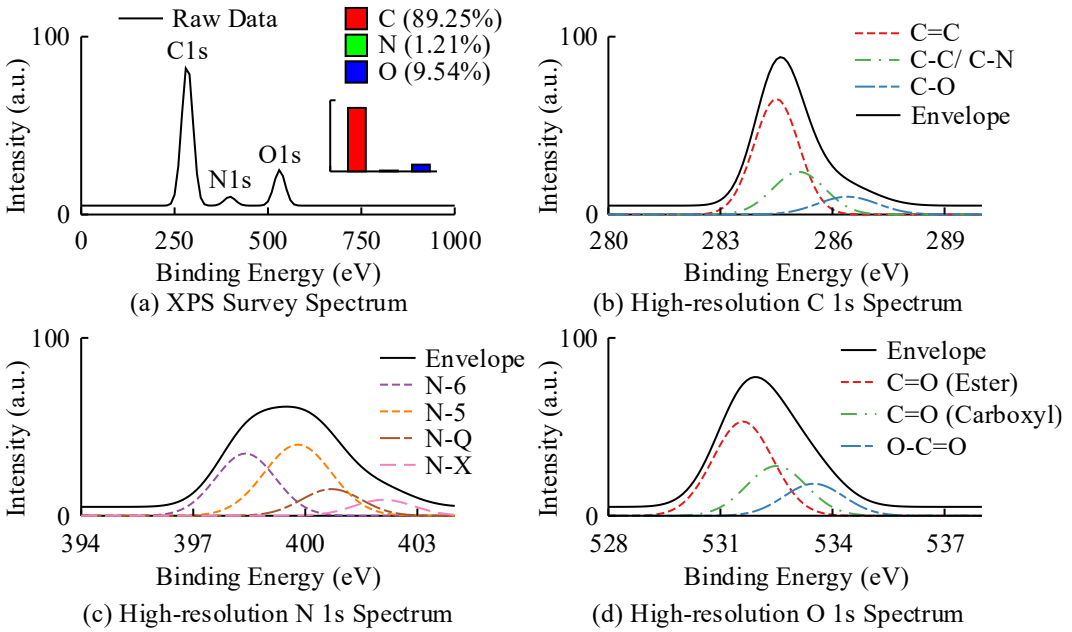

Fig.8 XPS testing of PUC series PC

Fig.8 shows the composition of PUC surface functional groups through XPS testing. In Fig.8(a), the XPS full spectrum of the PUC sample clearly shows the feature peaks of C 1s, N 1s and O 1s. The embedded atomic proportion diagram shows that C element is absolutely dominant, accounting for 89.25%, and the surface contains an appropriate amount of O and a small amount of N elements. The C 1s high-resolution spectrum in Fig.7(b) can be fitted to three chemical bonds: C=C, C-C/C-N, and C-O. The C=C bond peak intensity representing the graphite-like structure is the highest, indicating that the material has an intrinsic conductive skeleton. In Fig.7(c), the N 1s spectrum is resolved into N-6, N-5, N-Q, and N-X. Various configurations of N doping help improve the surface hydrophilicity of carbon materials and provide additional active sites. In Fig.8(d), the O 1s spectrum is mainly composed of ester group C=O, carboxyl C=O, and O-C=O, and the ester group C=O is dominant. PUC PC has a stable carbon skeleton, and its surface is rich in N and O heteroatom functional groups, which can effectively enhance the electrolyte wettability.

3.3.2 Electrochemical performance evaluation

In Fig.9(a), as the current density grows from 1 to 20 $A \cdot g^{-1}$, the SC of each sample decreases. PUC-850 has the best rate performance and the highest initial SC, reaching 280 $F \cdot g^{-1}$, and its SC is 205 $F \cdot g^{-1}$ at a high current of 20 $A \cdot g^{-1}$. PUC-650 drops to 102 F·g-1, indicating that moderately increased mesopores effectively reduces mass transfer resistance under high current. In Fig.9(b), at 10 $A \cdot g^{-1}$, the capacity retention rate (CRR) of PUC-850 reaches a peak of 85.4%, which is significantly better than the 58.9% at 600°C and 69.9% at 900°C. PUC-850 has the lowest initial ESR of only 0.97 Ω, which only slightly increases to 1.05 Ω after 10,000 cycles. The internal resistance of PUC-650 increases from 1.34 Ω to 1.85 Ω. At the carbonization temp of 850°C, the material's conductive skeleton and ion transmission channels can achieve an optimal balance.

Fig.10 is the SEM image and TEM image of PUC-850. In Fig.10(a), PUC-850 exhibits a coral-like 3D porous skeleton morphology. It is beneficial to promote the deep infiltration of

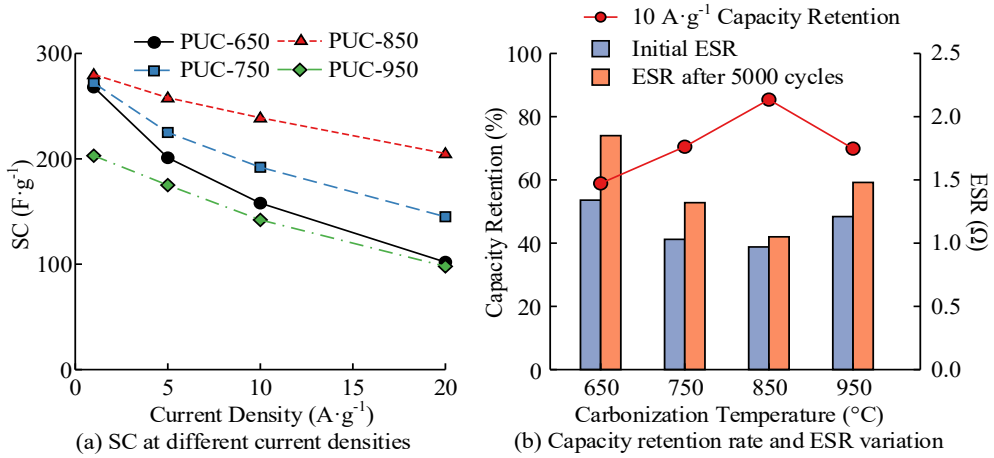

Fig.9 Electrochemical properties of PUC series PC

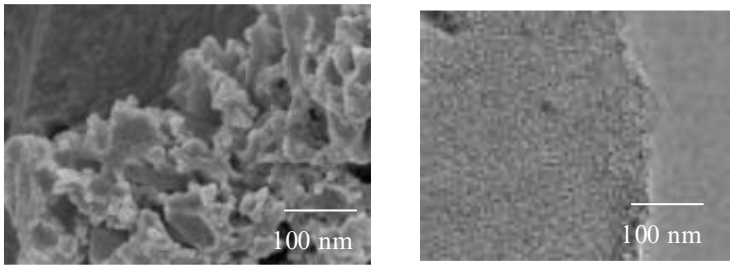

Fig.10 SEM and TEM images of PUC-850

electrolyte into the carbon material and reduce the DR-EI when rapidly charging and discharging. In Fig.10(b), the material substrate shows strong light transmittance, and its interior is densely distributed with tiny spots of light and dark. The matrix is highly disordered and typically amorphous. This is mainly attributed to the fact that the chemical etching of KOH activator breaks the original regular carbon crystal structure and introduces lots of lattice defects. Compared with highly graphitized carbon materials, this highly disordered amorphous carbon skeleton builds a richer open micropore and mesopore network in space, which greatly shortens the transmission path of electrolyte ions. More importantly, the disorder of the amorphous structure means that there are many edge defects and coordination unsaturated sites on the surface of the material. These structural defects not only enhance the accessibility of electrolyte ions, but also act as highly active Faraday redox sites, inducing additional pseudocapacitive contributions. This is highly consistent logically with the high rate electrochemical characteristics.

3.4 Performance analysis of PFC

3.4.1 Pore structure and surface chemistry

In Fig.11(a), as the carbonization temp rises from 650 to 950 ℃, the SSA of the PFC series samples first increases and

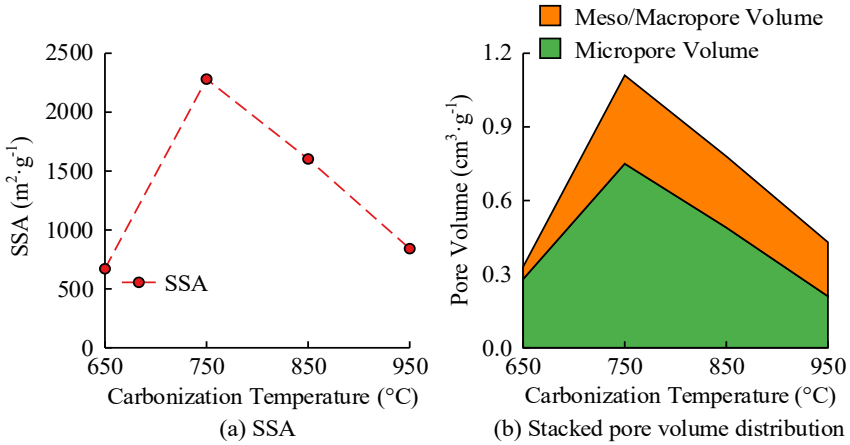

Fig.11 The influence of carbonization temp on the pore structure of PFC series PC

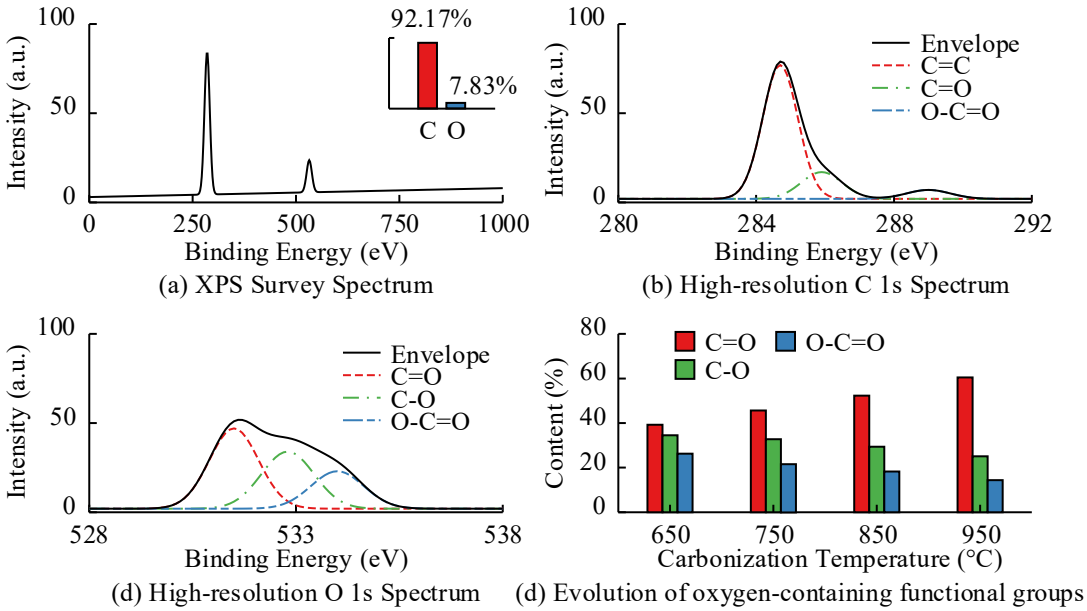

(a) XPS Survey Spectrum (b) High-resolution C 1s Spectrum
(d) High-resolution O 1s Spectrum (d) Evolution of oxygen-containing functional groups

Fig.12 XPS testing of PFC series PC

then decreases, arriving a peak of 2281 $m^2 \cdot g^{-1}$ at 750°C. When the temp continues to rise to 950°C, excessive etching causes severe collapse of the pore skeleton, and the SSA drops to 842 $m^2 \cdot g^{-1}$. In Fig.11(b), the evolution trends of micropore volume and meso/macropore volume are highly consistent with SSA. Both reach the maximum expansion at 750°C, up to 0.75 and 0.36 $cm^3 \cdot g^{-1}$, and then contracts simultaneously at high temps. 750°C is the optimal temp for the development of pores in PFC-derived PC. At this temp, it can effectively retain a large number of micropores, provide the largest electric double-layer energy storage area, and is conducive to building low-resistance ion transmission channels.

Fig.12 displays the effect of carbonization temp on the surface chemical properties of PFC series PC analyzed through XPS testing. In Fig.11(a), the PFC sample only shows C1s and O1s characteristic peaks, which is a typical N-free system. Embedded data show that the C element is as high as 92.17%, which is dominant. The C1s spectrum in Fig.12(b) shows that the C=C bond peak representing the graphitized structure has the highest intensity, indicating that the material has an intrinsic conductive skeleton. In Fig.12(c), the O1s spectrum is analyzed into three OCFGs: C=O, C-O and O-C=O. These polar groups can effectively improve electrolyte wettability and provide additional Faradaic pseudocapacitance. In Fig.12(d), as the activation temp rises from 650°C to 950°C, although the overall oxygen content of the material decreases, among the remaining oxygen species, the proportion of C=O with high thermal stability and high electrochemical activity increases significantly from 39.2% to 60.5%. The unstable C-O and O-C=O groups gradually decompose. 750°C helps optimize the PFC channel structure and achieve synergy between double-layer energy storage and pseudocapacitance.

3.4.2 Electrochemical performance evaluation

Fig.13 finally analyzes the comprehensive impact of preparation conditions on the electrochemical properties of PFC series PCs. In Fig.13(a), when the activation ratio is fixed at 1:3, the material's SC and CRR under high current both show a trend of first rising and then decreasing as the carbonization temp increases, and simultaneously reach the peak at 750°C, as high as 255 $F \cdot g^{-1}$ and 76.5%. When the temp continues to rise to 950°C, the carbon skeleton severely collapses, resulting in a large loss of energy storage sites, and all indicators drop

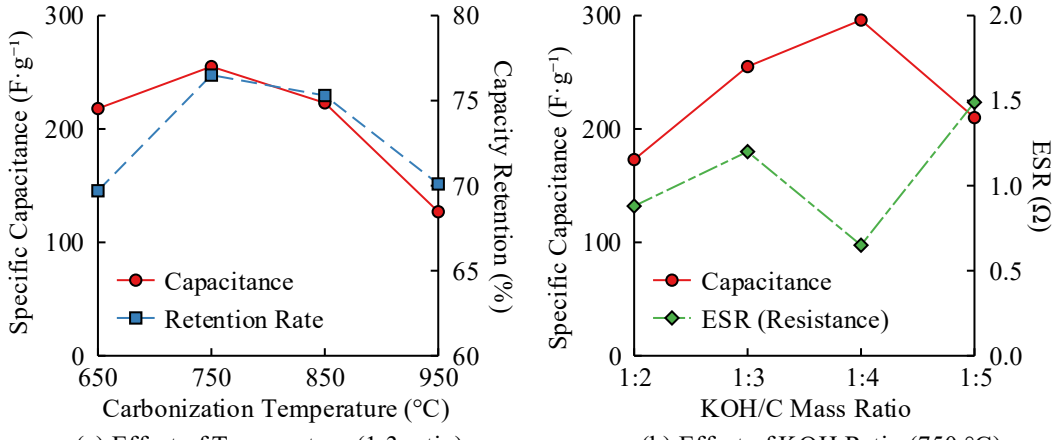

(a) Effect of Temperature (1:3 ratio) (b) Effect of KOH Ratio (750 °C)

Fig.13 Electrochemical properties of PFC series PC

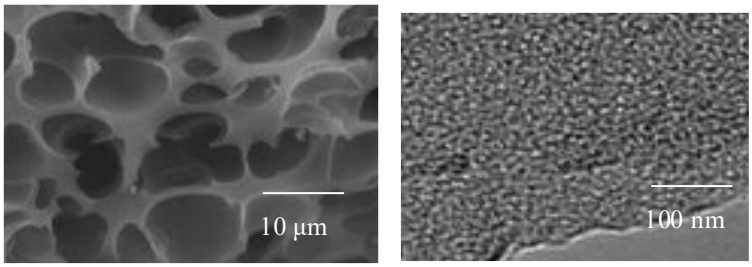

(a) SEM image (b) TEM image

Fig.14 SEM and TEM images of PFC750 (1:4)

significantly. In Fig.13(b), at a fixed 750℃, as the KOH/C mass ratio rises from 1:2 to 1:4, the SC of the material continues to increase to 296 $F \cdot g^{-1}$, and the ESR drops to the lowest point of 0.65 Ω at this ratio. When the activator ratio further increases to 1:5, excessive etching blocks the electron transmission channel, causing internal resistance to rebound and capacitance to decay. Therefore, 750℃ carbonization temp and 1:4 activation mass ratio are the best process combinations for PFC-derived PC.

Fig.14 is the SEM image and TEM image of PFC750 (1:4). The SEM image shows that the PFC750 (1:4) PC material exhibits a honeycomb-like 3D skeleton morphology. This type of pore framework is conducive to expanding the effective SSA of the material and promoting the rapid shuttle and transfer of electrolyte ions. The TEM image shows that the carbon layer of PFC-750 (1:4) exhibits excellent electron beam transmittance, and alternating light and dark spots are still densely distributed on the substrate. By statistically measuring the pore characteristics in TEM images, the size of the light and dark alternating micropores is mainly concentrated between 1.2-2.5 nm, and the pore wall thickness is about 3-5 carbon atom layers. There are short-range ordered worm-like carbon lattice stripes locally, and the measured interplanar spacing is about 0.36-0.38 nm. This value is significantly larger than the standard graphite's 0.335 nm, indicating that the structure is mainly composed of amorphous carbon while maintaining the basic graphitized conductive network. The expanded carbon interlayer spacing facilitates the rapid insertion and extraction of hydrated ions in the electrolyte. This shows that the material contains an extremely dense micro-nanoscale pore network.

3.5 Performance evaluation of symmetrical supercapacitors

To compensate for the shortcomings of the three-electrode system in reflecting the performance of actual energy storage devices, a symmetrical supercapacitor (SSC) based on HFC-750 (1:4) positive and negative electrodes is assembled. The study mainly introduces commercially available activated carbon (Commercial AC) and typical polymer derived PC (Other PC) as control benchmarks. Commercial AC selects representative high specific surface area benchmark activated carbon materials to simulate the actual application benchmark of current

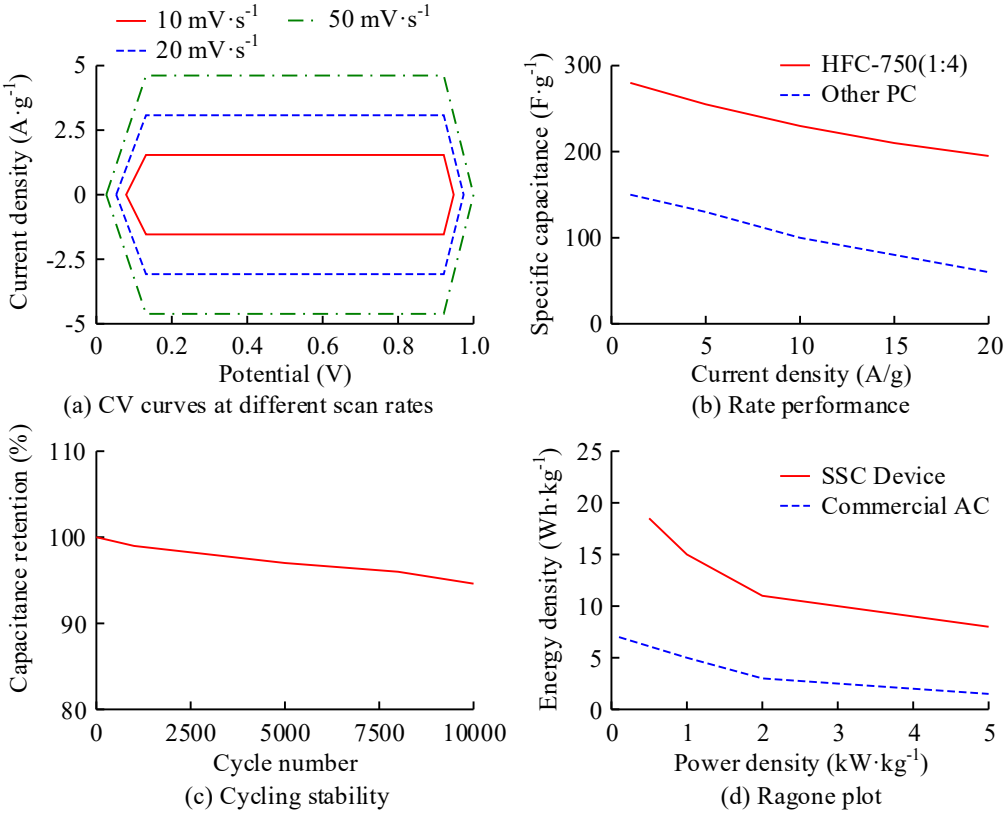

(a) CV curves at different scan rates (b) Rate performance

(c) Cycling stability (d) Ragone plot

Fig.15 Electrochemical performance of symmetrical SSC

industrial supercapacitors. The Other PC control group comes from recent research on high-performance waste polymer derived activated carbon, and its preparation follows a similar KOH HTA strategy. The electrochemical performance of symmetric SSC is shown in Fig.15. From Fig.15 (a), under the operating voltage window of 0-1.0 V, the SSC device exhibits a nearly rectangular cyclic voltammetry curve, demonstrating its excellent capacitance characteristics and device reversibility. Fig.15 (b) shows the constant current charge discharge curves at different current densities. Even at a high current density of 10 $A \cdot g^{-1}$, the specific capacity remains at 82% of its initial value, demonstrating excellent rate performance. Fig.15 (c) shows the long-term cycling stability of the device, with a capacitance retention rate of up to 94.6% after 10,000 GCD cycles, demonstrating excellent structural stability. The Ragone plot in Fig.15 (d) quantifies the energy density and power density of the device. The results show that the SSC device can achieve an energy density of 18.5 $Wh \cdot kg^{-1}$ at a power density of 0.5 $kW \cdot kg^{-1}$, which is superior to most carbon-based supercapacitors derived from waste polymers, demonstrating its practical application value as a high-performance energy storage device.

3.6 Electrochemical kinetics and analysis of pseudo capacitance contribution

To further confirm the synergistic pseudocapacitive effect induced by self-doping of heteroatoms, this study quantitatively analyzes the kinetic control process of the HFC-750 (1:4) electrode using the Dunns method, as shown in Fig.16. Fig.16(a) shows the ratio of capacitance control contribution to diffusion control contribution at different scanning rates. As the scanning rate increases from 2 $mV \cdot s^{-1}$ to 20 $mV \cdot s^{-1}$, the contribution rate of capacitor control increases from 62.4% to 84.7%. This indicates that in this material, the rapid charge adsorption at the interface and the surface Faraday redox reaction of functional groups within a short charge discharge time jointly constitute the main current response mechanism. In contrast, the capacitance contribution rate of pure carbon materials in the control group is only about 35%, showing a decreasing trend with increasing scan speed. It has been demonstrated that N and O heteroatom sites achieve in-situ enhancement of pseudocapacitance by reducing the charge transfer energy barrier. Fig.16(b) shows the distribution of capacitance contribution at 10 $mV \cdot s^{-1}$, with shaded areas representing the actual contribution of pseudo capacitance to the total current. Its high proportion of 76.2% quantitatively demonstrates the effectiveness of this strategy in achieving synergistic energy storage effects.

To ensure the statistical reliability of the test data, all electrochemical measurements are conducted in parallel on three independent button cell samples. The electrochemical performance comparison of activated carbon derived from different waste polymers is shown in Table 3. According to Table 3, statistical tests show that there are significant differences in the contribution of different precursors to the final product capacitance due to differences in their natural structure and self-doping microenvironment. The specific capacitance of PFC in the nitrogen free system is 315±10 $F \cdot g^{-1}$, which is not significantly different from the reference group (p>0.05). In contrast, PUC with a coral shaped three-dimensional porous skeleton shows significant performance improvement, with a specific capacitance of 342±11 $F \cdot g^{-1}$, and reaches a significant difference level compared to the baseline group (p<0.05). The

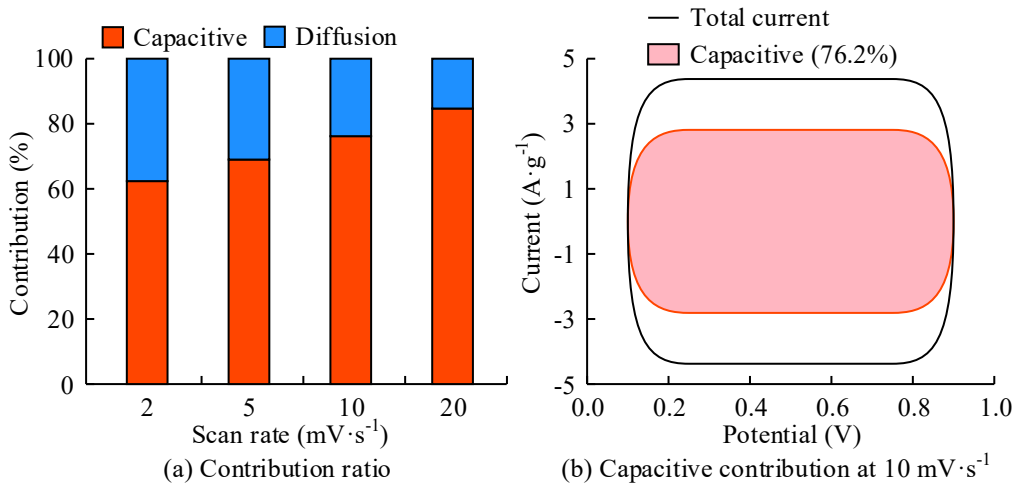

Fig.16 Quantitative analysis of dynamic control process

Table 3
Comparison of electrochemical properties and statistical significance of porous carbon derived from different waste materials

Source of materials	Activation method	SSA ($m^2 \cdot g^{-1}$)	Current density ($A \cdot g^{-1}$)	Specific capacitance ($F \cdot g^{-1}$)	Cycle stability	p
Waste plastic	KOH	1850±45	1.0	245±8	92.0%±1.2%	/
Polyurethane foam	$ZnCl_2$	2100±55	1.0	280±12	90.0%±1.5%	/
Waste tire rubber	KOH	2560±62	1.0	310±10	93.0%±0.8%	Reference group
PFC	KOH	2150 ± 38	1.0	315 ± 10	92.5% ± 0.7%	> 0.05
PUC	KOH	2420 ± 48	1.0	342 ± 11	93.8% ± 0.6%	< 0.05
HFC	KOH	2934 ± 52	1.0	385 ± 9	94.6% ± 0.5%	< 0.01

average specific capacitance of HFC materials with a hierarchical network of micropores and mesopores and the synergistic effect of high-density N/O active sites reaches 385±9 $F \cdot g^{-1}$, with a highly significant statistical difference (p<0.01). In addition, after 10,000 long cycles, the standard deviation of the three materials is controlled within ±0.7%. This series of derivatization processes endows the carbon matrix with excellent structural robustness while maintaining high reproducibility.

4. Discussion

To achieve high-value recycling and energy utilization of polymer waste, this study successfully converted HFC, PUC, and PFC into HPS electrode materials through pre-carbonization combined with KOH HTA strategy. For HFC, its SSA was 2,934 $m^2 \cdot g^{-1}$ at 750°C and a carbon-alkali ratio (CAR) of 1:4, and the starting SC reached 297 $F \cdot g^{-1}$. The SC of conventional biomass or coal-based PCs in the existing literature was usually between 150 and 250 $F \cdot g^{-1}$, and the rate performance at large currents was seriously attenuated (Hallad & Panwar 2026). In comparison, HFC materials showed huge capacity advantages. This is attributed to the synergistic mechanisms of both physics and chemistry. Physically, waste hollow fibers already have a tubular and fiber network that is conducive to fluid penetration. After intense chemical etching by KOH, it further evolved into a 3D interpenetrating network micro-mesoporous interconnected structure, thereby shortening the diffusion path of electrolyte ions. Chemically, the N-rich polymer precursor achieves in-situ self-doping of N and oxygen heteroatoms at 750°C, effectively superposing double-layer energy storage and pseudo capacitance. From the perspective of physical and chemical kinetics, this synergistic effect essentially stems from the scale matching effect and the reshaping of electronic band structure. The etching process of KOH inside the fiber skeleton follows a controlled thermodynamic evolution path. The inherent hollow structure of the fiber reduces the diffusion resistance of the activator to the microscopic interior, allowing the etching reaction to accurately induce the formation of gradient pore structures. In-situ doping of heteroatoms introduces high-density impurity states near the Fermi level, which enhances the delocalization ability of charge carriers and reduces the energy barrier for cross-interface electron transfer, constructing an efficient long-range charge transport pathway in the amorphous carbon skeleton.

For PUC, under HTA of 850°C, its SSA was as high as 1467 $m^2 \cdot g^{-1}$, the SC was 205 $F \cdot g^{-1}$ at a high current of 20 $A \cdot g^{-1}$, and the CRR at 10 $A \cdot g^{-1}$ was 85.4%. In previous studies, the pyrolysis of polyurethane polymers faced technical bottlenecks such as easy agglomeration of products, easy collapse of pores, and high internal resistance (Romero *et al.* 2024). The generated PUC had a coral-like rigid 3D skeleton, which promoted deep graphitization of the carbon skeleton, reducing the equivalent series internal resistance of the material to 0.97 Ω. This material was dominated by C=C bonds, which effectively buffers the volume stress during long-term charge and discharge processes. The enhancement mechanism of its conductivity lies in optimizing the conductivity penetration threshold caused by local crystallization. Unlike traditional disordered pyrolysis processes, the coral-like skeleton of PUC is formed at 850 °C, achieving ideal connectivity between microcrystalline and amorphous regions through internal short-range ordered rearrangement. This topology not only optimizes the charge transport percolation network but also induces a strong electric field concentration effect at the electrolyte/electrode interface due to its high curvature surface morphology.

For PFC, its SSA was 2,281 $m^2 \cdot g^{-1}$ at 750 °C, its SC was 296 $F \cdot g^{-1}$, and its ESR was only 0.65 Ω in large current and long cycles. Many studies have attempted to modify surface OCFGs through strong acid oxidation (Kadela *et al.* 2024), but such methods will cause large-scale damage to the carbon skeleton. The advantage of PFC was that its OCFGs were inherited in situ. Microscopic mechanism analysis showed that the activation temp of 750 °C promoted the formation of a honeycomb-like regular porous configuration of PFC. It maximized the double-layer energy storage interface and enriched the carbon surface with carbonyl and quinone groups with extremely high electrochemical activity. This phenomenon reflects the deep regulation of ion transport kinetics by the surface functional group confinement effect. The honeycomb skeleton of PFC is not a simple porous structure, and the curvature radius of its internal pore walls is on the same physical scale as the Debye length of hydrated ions. This scale matching effect greatly weakens the steric hindrance effect of the solvation shell. The carbonyl and quinone groups inherited in situ serve as typical Faraday active sites. Through electrochemical adsorption induced coordination modification, the electrostatic potential distribution on the pore surface is changed, thereby achieving rapid ion insertion and deintercalation in the double-layer charge balance process.

5. Conclusion

This study used pre-carbonization and KOH high-temperature chemical activation strategies to successfully convert HFC, PUC, and PFC into high-performance PC electrode materials. HFC had the best overall performance at 750°C and a CAR of 1:4, and still maintained a high capacity of 239 $F \cdot g^{-1}$ at 20 $A \cdot g^{-1}$. PUC formed a coral-like rigid 3D skeleton after HTA at 850 °C, with an SSA of 1467 $m^2 \cdot g^{-1}$, a capacity of up to 85.4% at 10 $A \cdot g^{-1}$, and an internal resistance of 0.97 Ω. At 750 °C and a CAR of 1:4, PFC had an ESR of 0.65 Ω under high current conditions, showing excellent electrochemical performance. As the temp increased, the N and O elements gradually decreased, and the PC material retained an appropriate amount of N and oxygen doping at 750 °C, which is beneficial to improving electrochemical activity. In addition, pore structure analysis showed that at 750 °C, the material had an effective pore expansion effect, could provide the maximum double-layer energy storage interface, and optimized the ion transmission path. In summary, the three prepared polymer waste-derived PCs had excellent electrochemical properties.

However, the KOH HTA process has strong equipment corrosion. Under existing experimental conditions, electrochemical performance evaluation is only limited to 6 M KOH aqueous electrolyte, which limits the further improvement of the voltage window and energy density. Therefore, future work should focus on developing greener and milder activators to replace the traditional strong alkali process and further explore the electrochemical performance in organic electrolytes.

References

Ahmad, F., Khan, M. A., Waqas, U., Ramay, S. M., & Atiq, S. (2023). Elucidating an efficient super-capacitive response of a $Sr_2Ni_2O_5$/rGO composite as an electrode material in supercapacitors. *RSC Advances*, 13(36), 25316-25326. https://doi.org/10.1039/D3RA03140C

Ashok Kumar, S. S., Bashir, S., Pershaanaa, M., Kamarulazam, F., Saidi, N. M., Goh, Z. L., … & Manikam, R. (2023). A review on the recent progress of the plant-based porous carbon materials as electrodes for high-performance supercapacitors. *Journal of Materials Science*, 58(15), 6516-6555. https://doi.org/10.1007/s10853-023-08413-7

Benoy, S. M., Hazarika, A., Bora, M., Rajbongshi, A., Sarmah, D., Phukan, M. K., & Saikia, B. K. (2024). Coal-derived porous carbon as versatile electrode materials for aqueous, water-in-salt, and organic electrolytes, and fabrication of pouch cell supercapacitor toward power application. *ACS Applied Energy Materials*, 7(15), 6045-6061. https://doi.org/10.1021/acsaem.4c01018

Blanchard, R., & Mekonnen, T. H. (2024). Valorization of plastic waste via chemical activation and carbonization into activated carbon for functional material applications. *RSC Applied Polymers*, 2(4), 557-582. https://doi.org/10.1039/d4lp00016a

Chen, S., & Hu, Y. H. (2025). All-plastic supercapacitors from poly (ethylene terephthalate) waste. *Energy & Fuels*, 39(37), 18128-18137. https://doi.org/10.1021/acs.energyfuels.5c03370

Ding, S., Xue, Y., Hu, H., & Wang, S. (2024). Pseudocapacitance-enhanced mesoporous carbon produced by stepwise pyrolysis of discarded oil-absorbing aerogels. *Energy & Fuels*, 38(17), 16520-16531. https://doi.org/10.1021/acs.energyfuels.4c02861

Hallad, S. C., & Panwar, N. L. (2026). Development of carbon electrodes and electrochemical double-layer supercapacitors using agricultural crop residue biomass-derived porous carbon. *Clean Energy*, 10(1), 15-28. https://doi.org/10.1093/ce/zkaf057

Kadela, K., Grzybek, G., Kotarba, A., & Stelmachowski, P. (2024). Enhancing graphene nanoplatelet reactivity through low-temperature plasma modification. *ACS Applied Materials & Interfaces*, 16(15), 19771-19779. https://doi.org/10.1021/acsami.4c01226

Kushwaha, V., Mandal, K. D., Gupta, A., & Singh, P. (2024). $Ni_{0.5}Co_{0.5}S$ nano-chains: a high-performing intercalating pseudocapacitive electrode in asymmetric supercapacitor (ASC) mode for the development of large-scale energy storage devices. *Dalton Transactions*, 53(12), 5435-5452. https://doi.org/10.1039/D3DT04184K

Li, J., Wen, Y., Li, X., Zhang, H., Wang, H., Li, B., ... & Song, W. (2025). Porous Carbon from Hyper-cross-linked Polymers: A Cost-Effective Approach for Supercapacitors. *Langmuir*, 41(47), 31720-31742. https://doi.org/10.1021/acs.langmuir.5c02495

Li, J., Zhang, S., Hua, Y., Wen, X., Mijowska, E., … & Ruoff, R. S. (2024). Facile synthesis of accordion-like porous carbon from waste PET bottles-based MIL-53 (Al) and its application for high-performance Zn-ion capacitor. *Green Energy & Environment*, 9(7), 1138-1150. https://doi.org/10.1016/j.gee.2023.01.002

Li, K., Liu, Z., Ma, X., Feng, Q., Wang, D., & Ma, D. (2023). Different pretreatment methods combined with subsequent activation to convert waste eucalyptus bark into porous carbon electrode materials for supercapacitors. *New Journal of Chemistry*, 47(11), 5316-5329. https://doi.org/10.1039/D2NJ06060D

Ma, M., Liu, J., Huan, Y., Ren, M., Wei, T., & Yan, S. (2024). Nitrogen-doped hierarchical nanoporous carbon materials from discarded polyurethane sponges via one-step double-activation method for double-layer capacitors. *ACS Applied Nano Materials*, 7(3), 2879-2888. https://doi.org/10.1021/acsanm.3c05153

Niu, Y., Gao, P., Ju, S., Li, F., Wang, S., Xu, Z., … & Peng, H. (2023). Hydrogen peroxide/phosphoric acid modification of hydrochars for sulfamethoxazole and carbamazepine adsorption: the role of oxygen-containing functional groups. *Langmuir*, 39(16), 5679-5688. https://doi.org/10.1021/acs.langmuir.2c03353

Ren, X., Li, M., Qiu, L., Guo, X., Tian, F., Han, G., … & Yu, Y. (2023). Cationic vacancies and interface engineering on crystalline–amorphous gamma-phase Ni–Co oxyhydroxides achieve ultrahigh mass/areal/volumetric energy density flexible all-solid-state asymmetric supercapacitor. *Journal of Materials Chemistry A*, 11(11), 5754-5765. https://doi.org/10.1039/D2TA09035J

Romero, C., Liu, Z., Wei, Z., & Fei, L. (2024). A review of hierarchical porous carbon derived from various 3D printing techniques. *Nanoscale*, 16(26), 12274-12286. https://doi.org/10.1039/D4NR00401A

Singh, P., Sharma, S., & Dhanorkar, M. (2023). Aquatic plant biomass-derived porous carbon: biomaterials for sustainable waste management and climate change mitigation. *International Journal of Environmental Science and Technology*, 20(11), 12955-12970. https://doi.org/10.1007/s13762-022-04601-1

Sun, J., Zhang, D., Zhang, R., Zhang, J., Zhao, Q., He, H., … & Xu, Y. (2024). Novel polyurethane based, fully flexible, high-performance piezoresistive sensor for real-time pressure monitoring. *ACS Applied Materials & Interfaces*, 16(19), 25422-25431. https://doi.org/10.1021/acsami.4c05098

Taer, E., Apriwandi, A., & Taslim, R. (2025). Heteroatom-doped biomass-derived porous carbon for supercapacitor applications: A review. *Trends in Sciences*, 22(8), 10115-10115. https://doi.org/10.48048/tis.2025.10115

Tian, L., Zhi, Y., Yu, Q., Xu, Q., Demir, M., Colak, S. G., … & Hu, X. (2024). Enhanced CO_2 adsorption capacity in highly porous carbon materials derived from melamine-formaldehyde resin. *Energy & Fuels*, 38(14), 13186-13195. https://doi.org/10.1021/acs.energyfuels.4c02372

Wang, K., Li, R., Zeng, X., Song, P., Sun, J., & Song, R. (2025). Converting waste poly (ethylene terephthalate) into hierarchical porous carbon towards a high-performance supercapacitor. *Journal of Materials Chemistry A*, 13(10), 7381-7391. https://doi.org/10.1039/d4ta08522a

Wang, Z., Gao, L., Zhong, X., Zhang, Y., Shakeri, M., Zhang, X., & Zhang, B. (2025). Accurately tuning the pore size and acidity of mesoporous zeolites for enhancing the catalytic hydrocracking of polypropylene. *Journal of Materials Chemistry A*, 13(4), 2875-2883. https://doi.org/10.1039/D4TA07329K

Yue, M., Lu, H., & Liu, H. (2025). Study on the preparation of biomass-derived porous carbon and enhanced carbon capture performance via MOF-assisted granulation. *Langmuir*, 41(19), 12078-12088. https://doi.org/10.1021/acs.langmuir.5c00804

Zhou, S., Xu, Q., Zhong, X., & Hu, X. (2026). Activated Carbon from KOH-Activation of the Polymeric Product from Cross-Polymerization of Bio-Oil and Furfural as Electrode Material of Supercapacitors. *Waste and Biomass Valorization*, 17(1), 257-269. https://doi.org/10.1007/s12649-025-03121-6